Application of automated corrosion sensors for monitoring the rate of corrosion during accelerated corrosion tests

T. Prosek*, N. Le Bozec and D. Thierry

An automated corrosion monitoring system using the electrical resistance technique was applied for assessment of the corrosivity towards carbon steel and zinc in different phases of a complex accelerated corrosion test recently introduced by VDA, an association of German car makers. It comprises salt spray, wet, dry, and freezing phases. The developed small and battery-driven atmospheric corrosion loggers provided high sensitivity allowing for sub-angstrom ($<10^{-10}$ m) measurements of corrosion depth and good accuracy. The actual corrosion rate was affected by the exposure history due to a limited rate of wetting/drying and oxygen and ion transport to the reaction interface under a layer of corrosion products. The hysteresis was particularly strong for carbon steel. Except the freezing phase, the steel corrosion rate varied in a narrow range from 0.2 to 0.6 μm/h. For zinc, the corrosion rate varied from 0.001 to 0.1 μm/h in particular phases of the cycle with the maximum in the salt spray phase. Seventy-five percent of the metal corroded in the salt spray phase and in the following drying period representing only 13% of the total test time. The obtained data suggest that the proposed test cycle allowed for rather efficient drying of the zinc surface, which is believed to be crucial for the formation of corrosion products with certain protective ability observed also in field conditions.

1 Introduction

Whereas there is a relatively wide range of products for corrosion monitoring in aqueous media, the availability of means for real-time corrosion monitoring in the atmosphere is limited. A quartz crystal microbalance (QCM) measures corrosion through changes in the resonance frequency of a piezo electric quartz crystal coated with a thin metallic layer, the resonance frequency being a function of the mass of the crystal [1, 2]. This technique, based on evaluation of mass gain of the metal coating during the corrosion process, can be applied to monitor corrosivity under mild atmospheric conditions [3]. A disadvantage of this method is that it is equally sensitive to any mass gain, e.g. from dust and other contaminants, as to the formation of corrosion products. Further, water is adsorbed on the surface, and its amount depends on the relative humidity, metal, surface roughness and surface film present [4]. These facts limit the technique for applications in low corrosive environments.

T. Prosek, N. Le Bozec, D. Thierry
French Corrosion Institute, 220 rue Pierre Rivoalon, 29200 Brest (France)
E-mail: tomas.prosek@institut-corrosion.fr

Several techniques for corrosion monitoring by optical means have been proposed. A metal clad optical sensor is formed from a standard multimode optical fiber where the plastic cladding is replaced by a metal film. The metal cladding increases radiation losses, since the fiber is no longer a wave-guide in the metal-coated region. As the metal oxidizes, light losses decrease and the output power from the optical fiber increases [1, 5]. However, there is not yet any commercial product based on the optical methods on the market.

Ultrasonic testing is a well-established non-destructive technique used to control the corrosion state of metallic structures. It consists in generating an acoustic wave that propagates in the tested material and in recording reflections returning from the surface of the objects or from internal heterogeneities. The accuracy in field conditions is usually limited to a few hundreds of micrometers on corroded materials [6], but better results can be obtained in laboratory conditions [7, 8]. The drawback of the technique is that it is sensitive to the ultrasonic properties of specific corrosion products [8]. Further, it can be applied only for steel objects.

An interesting alternative to the traditional coupon technique and methods discussed above is the electrical resistance (ER) technique described for instance in standards ASTM G96 and ISO 11844–2 [9, 10]. The principle of the method is that ER of a

measuring element made from the material of interest increases as its cross sectional area diminishes due to corrosion. In practice, two such elements are built into a probe. One is exposed to the corrosive environment and corrodes whereas the other is shielded and thus protected from corrosion. The resistance is measured at the same time and resistivity changes due to temperature difference are compensated. Based on the initial cross-sectional area of the exposed element, the cumulative metal loss at the time of reading is determined. The benefits of the ER technique include its versatile nature; the technique can be used in practically any kind of environment with any material corroding about uniformly.

The ER monitoring system AirCorr^{TM} has been developed within European projects [11–13]. It exists in two basic variants designed for low corrosive environments where the sensitivity is crucial and for highly corrosive applications where robustness and water tightness are of the utmost importance. The former system was applied for monitoring in indoor cultural heritage premises where sub-angstrom ($<10^{-10}$ m) sensitivity was reached using thin copper, silver, lead, iron and bronze sensors with thicknesses from 50 to 800 nm [14, 15]. The latter set-up was used on operating vehicles in order to assess the corrosion aggressiveness towards steel and zinc as a function of locations on vehicle and thus possibly adapt the corrosion protection [16]. The corrosion loggers were successfully applied also in extreme corrosive environments represented by outdoor locations on operating ships such as a container carrier navigating between Europe and China [17].

The aim of this study was to monitor the corrosion rate of carbon steel and zinc during a complex accelerated corrosion test including wet, dry and salt spray phases. Hence, the influence of the different phases on the corrosion rate during the accelerated corrosion test could be studied.

2 Experimental

2.1 AirCorr corrosion loggers

The concept of the applied corrosion monitoring system is simple: the electronic unit measures and registers the change over time of ER of a thin metal track applied on an insulating substrate. If the metal corrodes, the cross-sectional area of the track decreases and the ER increases. A part of the metal track is protected by an organic coating or tape and, thus, serves as a reference to compensate for resistivity changes due to varying temperature. A schematic drawing and photograph of the sensor is shown in Fig. 1. This geometry ensures high sensitivity to changes in the ER due to metal corrosion.

The corrosion depth (CD) of the metallic sensor is calculated according to equation

$$\mathrm{CD} = t_{\mathrm{init}}\left(\frac{R_{\mathrm{ref,init}}}{R_{\mathrm{sens,init}}} - \frac{R_{\mathrm{ref}}}{R_{\mathrm{sens}}}\right) \quad (1)$$

where t_{init} is the initial thickness of the reference metallic track, which is assumed equal to the sensor track in the beginning of exposure, R_{sens} and R_{ref} are the actual ERs of the sensor and reference tracks, and $R_{\mathrm{sens,init}}$ and $R_{\mathrm{ref,init}}$ are the initial ERs of the sensor and reference tracks. The calculation is based on the ERs measured as a potential difference along the track through which defined currents pass [18, 19].

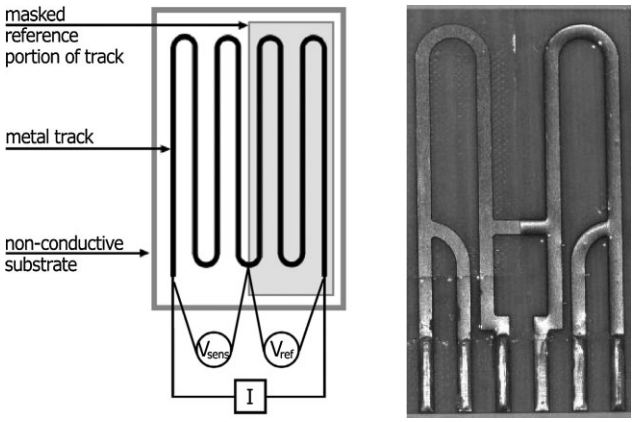

Figure 1. Schematic drawing of corrosion sensor (left) and photograph of Fe-250 μm sensor (right)

The changes in ER are recorded by a precise miniature electronic logger. For purpose of this study, watertight AirCorr O logger of $100 \times 65 \times 37\ \mathrm{mm}^3$ with a tightness of IP 65 designed for highly corrosive environments was used, see Fig. 2. The attached sensor is protected with a robust polyurethane casting and can be replaced when reaching the end of the life. The cadence of the measurement can be adjusted from minutes, to hours, to even days if necessary in order to match the sensitivity of the measurement with the anticipated corrosion rate. It was set to 5 min in this study. Details about reproducibility, sensitivity and accuracy of the technique can be found in reference [14].

2.2 Accelerated corrosion test

Among accelerated corrosion tests that are used by the automotive makers, the so-called N-VDA test was selected to

Figure 2. Photograph of watertight AirCorr O logger with mounted Fe-250 μm sensor for heavy corrosive environments

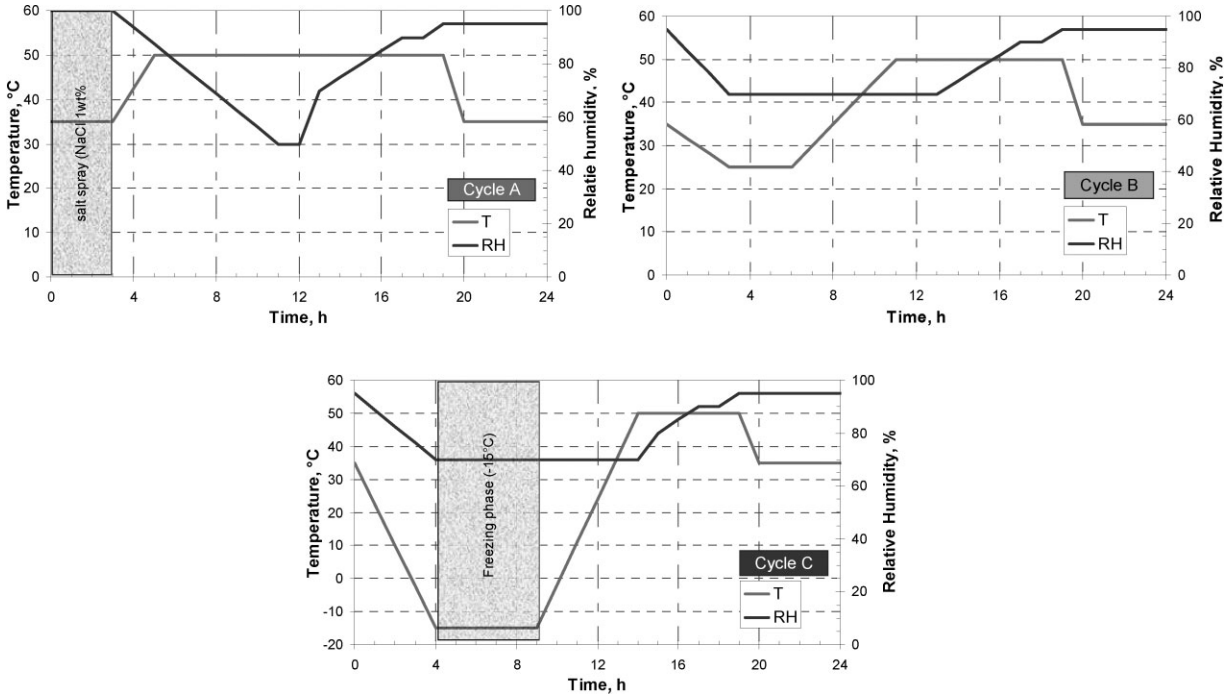

Figure 3. Sub-cycles of N-VDA test

evaluate the robustness of AirCorr O loggers. It should be mentioned that the N-VDA test, which is currently in development by a working group of the VDA (German vehicle producers association) and the VDEh (German steel producers association) as VDA 233-102 shall replace the test standard VDA 621-415 [20], indeed known to fail in simulating on vehicle exposures [20–23]. The N-VDA test was selected for this study because it includes a variety of technical phases such as a salt spray phase (NaCl 1 wt%, pH neutral), wet and dry cycles at several temperatures up to 50 °C and a freezing phase at −15 °C. It consists of three sub-cycles A, B, and C, with duration of 24 h each, as shown in Fig. 3. In a week cycle, the sub-cycles are ordered as A–B–A–C–A–B–B or B–A–C–A–B–B–A. A typical duration of the test is 6 weeks.

2.3 Experimental procedure

Since the corrosion logger is independent of any power supply, it was placed directly in a test chamber. Two steel sensors with the metal track layer thickness of 250 μm (Fe-250μm) and two zinc sensors of 25 μm (Zn-25μm) were consequently exposed. Loggers were placed with the longer sensor side parallel to the ground and with the protected part above the sensing part. In this position, water cannot accumulate on the sensing part. The sensor was oriented at 20° to vertical. In parallel, three zinc (99.99%) and carbon steel coupons were exposed to the chamber at the same angle. On completion of the exposure, collected and stored data were downloaded from the logger to a computer by a non-contact inductive data reader and evaluated using dedicated software. The mass loss of zinc and steel coupons was measured according to ISO 8407 after respective removal of corrosion products in glycine (250 g/L $C_2H_5NO_2$) and Clark's (1 L HCl, 20 g Sb_2O_3, 50 g $SnCl_2$) water solutions at room temperature.

3 Results and discussion

3.1 Zinc

Records of CD registered by two loggers with fresh sensors, L1 and L2, during three consecutive week cycles, C1, C2, and C3, are plotted in Fig. 4. Logger L2 was removed during the second cycle and logger L1 in cycle C3.

CD records from initial cycles C1 differed somewhat from those from the following cycles. A layer of corrosion products formed on the fresh sensor surface. After the initial corrosion product build-up in the first sub-cycles B and A corresponding to about 1.5 μm in CD, the corrosion rate dropped.

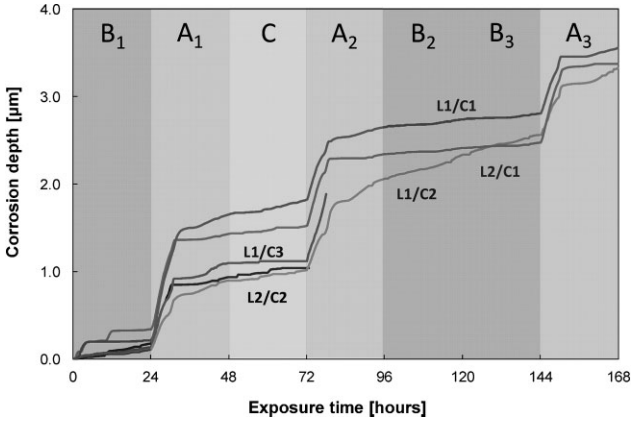

Figure 4. Record of CD measurements with Zn-25 μm sensors in N-VDA; L1, L2: Two parallel loggers/sensors; C1, C2, C3: 1st, 2nd, and 3rd week cycle of the test

Table 1. Changes in CD in sub-cycles of N-VDA measured with Zn-25 μm sensors (in μm)

Logger/cycle	Sub-cycle[a]							Full cycle
	B_1	A_1	C	A_2	B_2	B_3	A_3	
L1/C1	0.2	1.4	0.2	0.8	0.1	0.1	0.8	3.6
L2/C1	0.3	1.1	0.1	0.8	0.1	0.1	0.9	3.4
L1/C2	0.1	0.8	0.1	1.0	0.3	0.2	0.8	3.3
L2/C2	0.2	0.7	0.1	–	–	–	–	–
L1/C3	0.1	1.0	0.2	–	–	–	–	–
Average	0.1[b]	0.8[b]	0.1	0.9	0.1	0.1	0.8	3.4
Standard deviation	0.0[b]	0.1[b]	0.1	0.1	0.1	0.1	0.1	0.1

[a]Index gives an order of the sub-cycle in a week cycle;
[b]L1/C1 and L2/C1 are excluded because of the initial formation of corrosion products.

The CD measured in three complete cycles L1/C1, L2/C1, and L1/C2 was 3.6, 3.4, and 3.3 μm, respectively. It gives the average CD of 3.4 ± 0.1 μm. The relative standard deviation of 4% shows a very good reproducibility of the measurement. The obtained CD can be compared to the total mean zinc CD estimated from mass loss of zinc coupons exposed in the test for 6 weeks. It was 16.3 ± 2.4 μm, which corresponds to 2.7 μm/week if a constant rate of the corrosion process is expected from cycle 1 to cycle 6. The sensors showed 27% higher CD than coupons. It is not surprising because the ER technique measures in its principle a maximal depth of attack, whereas the coupon technique assesses an average depth. The maximal depth of corrosion is important from the practical point of view and often followed as the main parameter defining corrosion degradation of automotive materials [21, 24, 25]. In reality, the difference between the coupon and ER measurements is probably even smaller due to the fact that the corrosion rate of zinc usually tends to somewhat decrease in time due to a weak inhibiting effect of formed corrosion products and the CD in the initial cycles was thus probably higher than that calculated as 1/6 of the total in 6 weeks. Further difference in corrosion properties of bulk and thin film materials may come from different metallurgy. Anyway, it can be concluded that the two measurement techniques gave comparable results.

Changes in CD per sub-cycle are given in Table 1. It is evident that the most corrosive phases were sub-cycles A comprising the surface contamination with a solution of 1 wt% sodium chloride in a form of salt spray. The average increase in CD recorded in sub-cycles A in the 2nd and 3rd cycle of N-VDA (C2, C3) was 0.8 ± 0.1 μm. It was significantly lower in sub-cycles B and C, i.e. 0.1 ± 0.1 μm. Although a part of sub-cycle C is a freezing phase, the sub-cycles B and C were similar in terms of the corrosivity towards zinc.

The sub-cycles can be analyzed separately in detail as it is shown below for B_1 and A_1. CD, temperature and relative humidity records from the first B-sub-cycle, B_1, are seen in Fig. 5. The relative humidity and temperature records are from the 1st cycle C1. There was no principal difference between the RH and *T*-values measured in week cycles C1, C2, and C3. Corrosion of zinc initiated within less than an hour after the start of the test. The initial layer of corrosion products formed by corroding 0.2 μm of zinc at 25 °C and at 70% RH. In two cases, further activation was observed when the temperature reached 40 °C at the same RH.

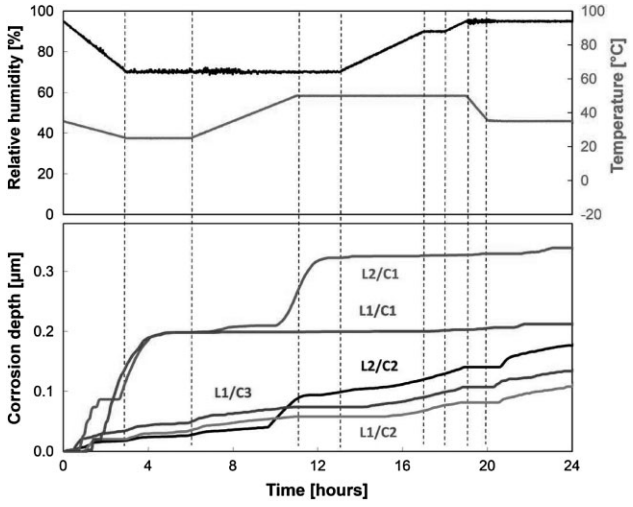

Figure 5. CD, temperature, and relative humidity measurements in sub-cycle B_1 with Zn-25 μm sensors

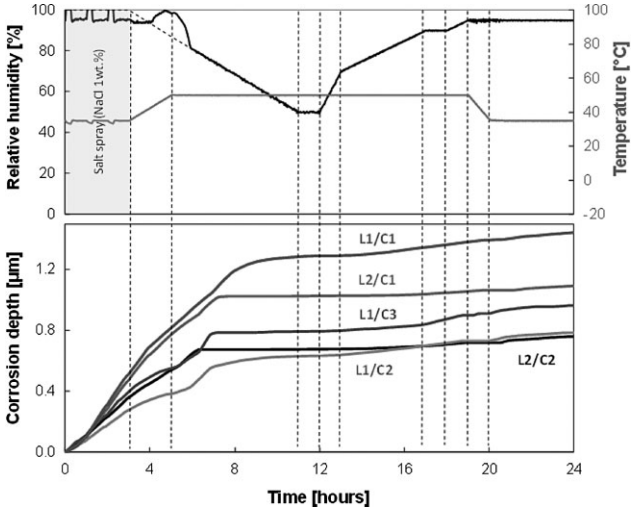

Figure 6. CD, temperature, and relative humidity measurements in sub-cycle A_1 with Zn-25 μm sensors; dashed line show desired RH

Table 2. Corrosion rate of zinc measured in periods with constant T and RH (in μm/h); average values for sensors with a developed layer of corrosion products

Conditions		Sub-cycle	Order of sub-cycle			Average
T [°C]	RH [%]		1	2	3	
35	100[a]	A	0.123	0.110	0.107	0.113
50	50	A	0.002	0.003	0.001	0.002
50	90	A	0.020	0.015	0.012	0.016
35	95	A	0.013	0.013	0.011	0.012
25	70	B	0.004	0.016	0.004	0.008
50	70	B	0.002	0.001	0.001	0.001
50	90	B	0.010	0.007	0.009	0.009
35	95	B	0.007	0.011	0.007	0.008
50	90	C	0.003	–	–	0.003
35	95	C	0.004	–	–	0.004

[a]Salt spray phase.

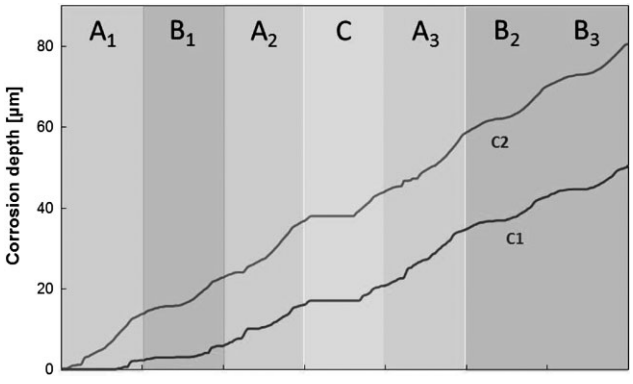

Figure 7. Record of CD measurement with Fe-250 μm sensor in N-VDA in modification A–B–A–C–A–B–B (L1); C1, C2: 1st and 2nd week cycle of the test

A similar record for sub-cycle A_1 is seen in Fig. 6. The corrosion rate increased immediately after the application of sodium chloride solution by spraying. During the salt spray phase, it kept at 0.11 ± 0.01 μm/h in sub-cycles A_1, A_2, and A_3 on pre-corroded surfaces. Thus, the process was reproducible. The corrosion rate only decreased slightly in the following phase when the temperature increased from 35 to 50 °C. It dropped when the relative humidity got below about 75% (ranging from 78 to 71% for particular cycles and sensors). It was relatively low in the rest of the sub-cycle.

Corrosion rates of zinc were extracted from the changes in CD in periods when both temperature and relative humidity were constant. They are given in Table 2. Obviously, there is a tendency to induce a higher corrosion rate at elevated temperatures and higher relative humidity. However, variations in the corrosion rate measured at identical RH and T in sub-cycles A, B, and C can be observed. For example, the corrosion rate at 50 °C and at 90% RH was 0.016 ± 0.004, 0.009 ± 0.002 and 0.003 μm/h in the respective sub-cycles. This emphasizes the fact that the rate of the corrosion process, taking place on the metal surface under a layer of corrosion products does not immediately reflect the actual climatic conditions. In particular, the drying and wetting process can be slow. It may take significantly longer than an hour until equilibrium is established between the atmosphere and the corroding system. The actual amount of water, chloride and other species available at the metal surface that control the surface chemistry and the corrosion process was besides the actual climatic and pollution characteristics affected also by the exposure history.

3.2 Carbon steel

Steel sensors of 250 μm were exposed to test cycles comprising sub-cycles A–B–A–C–A–B–B (L1) and B–A–C–A–B–B–A (L2). The aim was to investigate if an order of sub-cycles affects the total CD of carbon steel. Two week cycles of L1 were performed, denominated as L1/C1 and L1/C2. A single week cycle was carried out for L2, L2/C1.

Records of CD measured in L1 and L2 are displayed in Fig. 7 and in Fig. 8. It is interesting to notice that the corrosion of carbon steel did not initiate immediately. It took most of the first sub-cycle of 24 h to initiate the corrosion process, even when it was the sub-cycle A with the salt spray phase in L1. Consequently, the first and second cycle C1 and C2 in L1 differed in total CD. It was 51 and 81 μm, respectively. CD measured in the first week in L1 and L2 differing in the order of sub-cycles was however identical, 51 μm.

The CD measured using the automated sensors can be compared to that calculated from mass loss of carbon steel coupons. They were exposed for 1 and for 6 weeks in L2. The mean CD was 32 ± 3 and 254 ± 21 μm, respectively. When the depth obtained in 6 weeks is recalculated to 1 week, it gives 42 ± 4 μm. The maximal depth of corrosion attack was measured on the coupons exposed for 1 week using a micrometer gauge. It was found to be 80 ± 30 μm. Obviously, the depth measured by the sensors was higher than the mean depth calculated from the mass loss and within the maximal depth measured using a gauge.

CDs recorded in particular sub-cycles in L1 and L2 tests are given in Tables 3 and 4. Two principal observations can be made when the data are compared to those obtained for zinc. First, there were smaller differences in corrosion rates measured in particular sub-cycles for steel than for zinc. The average change in

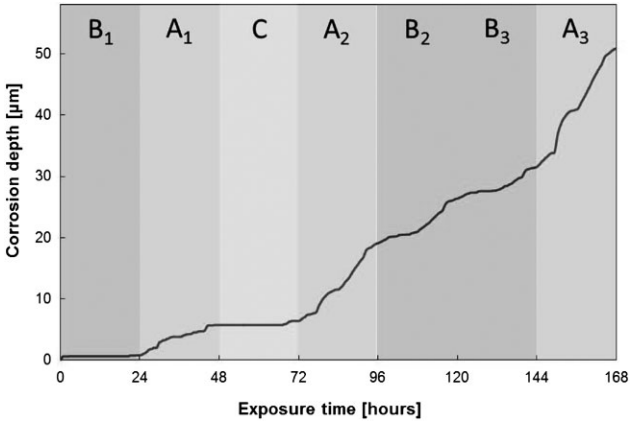

Figure 8. Record of CD measurement with Fe-250 μm sensor in N-VDA in modification B–A–C–A–B–B–A (L2)

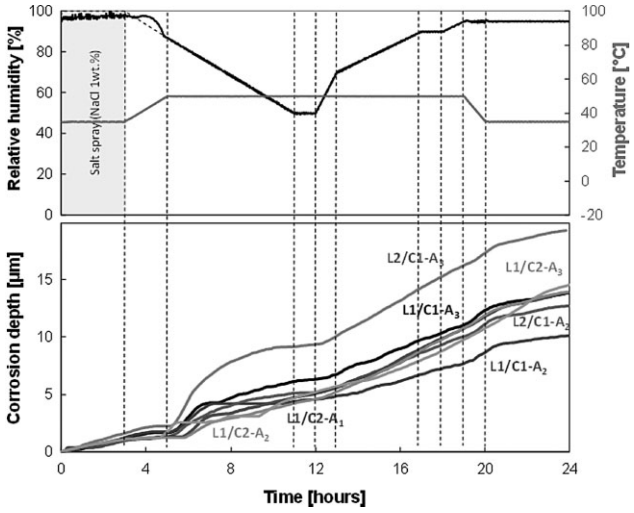

Figure 9. CD, temperature, and relative humidity measurements in sub-cycles A with Fe-250 μm sensors; dashed line show desired RH

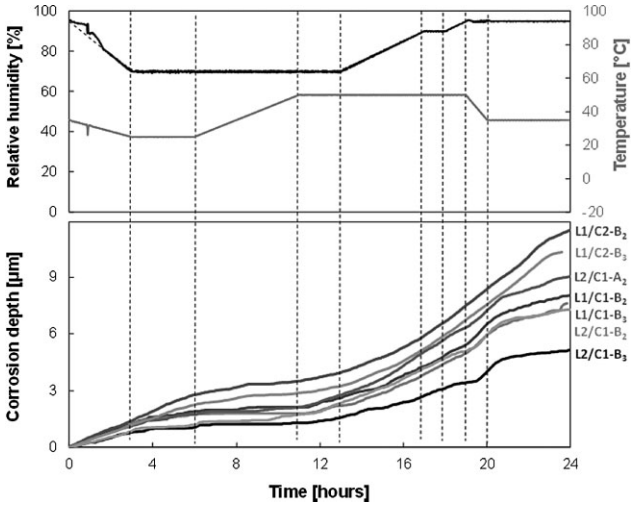

Figure 10. CD, temperature, and relative humidity measurements in sub-cycles B with Fe-250 μm sensors; dashed line show desired RH

CD in sub-cycles A, B, and C was 13 ± 5, 8 ± 3 and 4 ± 3 μm. Thus, the most corrosive sub-cycle A caused about 3-fold larger increase in the CD than the least corrosive sub-cycle C and the difference to sub-cycle B was of only 40%. For zinc, 6-fold difference was observed between sub-cycles A and both B and C. Second, the corrosivity in particular sub-cycles of the same type varied according to their order. For example, the first, second and third sub-cycle B in L1/C1 gave changes in the CD with the standard deviation of 40%. Both these observations indicate that the atmospheric corrosion of carbon steel was even less sensitive to actual bulk climatic conditions than that of zinc under conditions of this study. The strong hysteresis of the corroding system is expected to be due to slow changes in the conditions at the metal/corrosion product interface. Both the drying of corrosion products and transport of activators towards and from the interface are slow processes. In addition, the corrosion products on steel contain both Fe^{2+} and Fe^{3+} species, which makes the system less dependent on the actual availability of oxygen on the surface. Fe^{3+} species can reduce to Fe^{2+} replacing thus oxygen in the depolarization reaction [26].

Changes in CD and relative humidity and temperature records for sub-cycle A are plotted in Fig. 9. Corrosion rates in periods characterized by constant RH and temperature are given in Table 5. Excluded are first A-sub-cycles for L1/C1 and L2/C1 where lower CDs were measured due to incomplete activation of the surface. The corrosion rate was about 0.4 μm/h in the salt spray phase at 35 °C. It increased sharply during a drying phase at 50 °C when the relative humidity dropped under about 83–87%. A corrosion rate of about 2 μm/h was registered. It decreased when RH reached 73–76%. Thus, the maximal corrosion rate of steel was found after the salt spray cycle at the elevated temperature of 50 °C and the relative humidity between 75 and 85%. At around 80% RH, the surface is covered with a thin and continuous layer of water solution that enables for efficient transport of oxygen and

Table 3. Changes in CD in sub-cycles of N-VDA in modification L1 measured with Fe-250 μm sensor (in μm)

Cycle	Sub-cycle[a]							
	A_1	B_1	A_2	C_1	A_3	B_2	B_3	Full cycle
C1	2	4	10	5	14	8	8	51
C2	14	9	14	7	15	12	10	81

[a]Index gives an order of the sub-cycle in a week cycle.

Table 4. Changes in CD in sub-cycles of N-VDA in modification L2 measured with Fe-250 μm sensor (in μm)

Cycle	Sub-cycle[a]							
	B_1	A_1	C	A_2	B_2	B_3	A_3	Full cycle
C1	1	5	1	13	7	5	19	51

[a]Index gives an order of the sub-cycle in a week cycle.

Table 5. Corrosion rate of carbon steel measured in periods with constant T and RH (in μm/h); average values for sensors with a developed layers of corrosion products

Conditions		Sub-cycle	Order of sub-cycle			Average
T [°C]	RH [%]		1	2	3	
35	100[a]	A	0.3	0.4	0.4	0.4
50	50	A	0.2	0.2	0.3	0.2
50	90	A	0.5	0.6	0.7	0.6
35	95	A	0.4	0.5	0.7	0.5
25	70	B	0.2	0.2	0.2	0.2
50	70	B	0.3	0.3	0.2	0.3
50	90	B	0.3	0.3	0.3	0.3
35	95	B	0.4	0.5	0.4	0.5
50	90	C	0.4	–	–	0.4
35	95	C	0.3	–	–	0.3

[a]Salt spray phase.

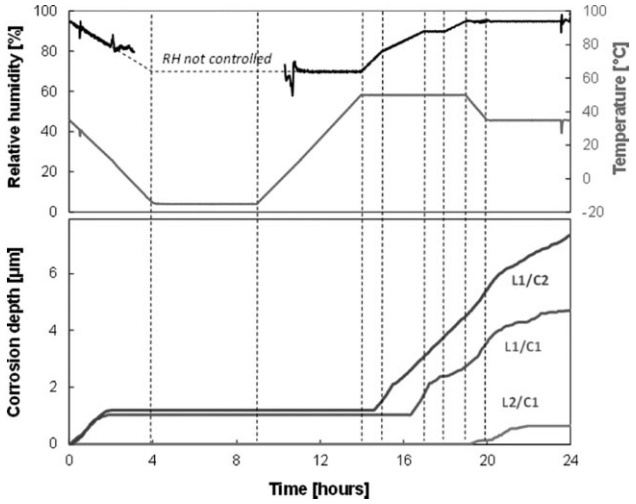

Figure 11. CD, temperature, and relative humidity measurements in sub-cycle C with Fe-250 µm sensors; dashed line show desired RH

ionic species [27]. The oxygen diffusion path is longer at higher RH and ionic transport is disrupted at lower RH. The corrosion rate in sub-cycle A was the lowest at 50 °C and 50% RH when it reached 0.2 µm/h. The highest corrosion rate was obtained at 50 °C and at 90% RH. It is in agreement to earlier measurements in a similar accelerated test using the ultrasonic technique [8].

It is interesting to note that the corrosion rate increased systematically from the first to the third sub-cycle, see Table 5. It indicates that not only the corrosion products formed on the surface had no protective ability but the corrosion process was accelerated underneath. It can be expected that local acidification and separation of anodic and cathodic locations was more efficient under a thicker layer of iron corrosion products.

No dramatic changes in the corrosion rate can be seen in the sub-cycle B (Fig. 10, Table 5). It decreased when the relative humidity dropped from 95 to 70%, then it started to increase when the temperature increased from 25 to 50 °C and decreased again at 35 °C. The highest corrosion rate was observed at 95% RH and 35 °C. It is interesting to note that the third B-sub-cycle was systematically less corrosive than the second one. It can be explained by a larger distance from sub-cycle A with the salt spray phase.

During the freezing phase in sub-cycle C, the corrosion rate was nil, see Fig. 11. It decreased sharply during cooling when the temperature got below about 15 °C. The corrosion process re-initiated when the relative humidity crossed 75% at 50 °C. Corrosion of the sensor used in cycle L2 initiated even later, when the relative humidity increased to 95%. This can be understood in view of the probabilistic nature of corrosion leading to somewhat different corrosion behavior of parallel identical samples.

3.3 Comparison of carbon steel and zinc degradation and implications for test development

Comparison of the data on corrosion rates in different phases of the test with constant conditions for zinc and carbon steel in Table 2 and Table 5 shows that the actual corrosion rate of carbon steel was less sensitive to conditions in the test chamber. Excluding the salt spray phase, it varied in a rather narrow range from 0.2 to 0.6 µm/h, whereas a variation from 0.001 to 0.012 µm/h was recorded for zinc. Even more striking difference between the materials is seen when the corrosivity within the salt spray phase is compared to the rest of the test. For carbon steel, it was only slightly elevated and periods with higher actual corrosion rates could be identified. For zinc, the salt spray phase constituted clearly a period of extreme changes in CD. In total, 75% of zinc corroded in this phase that took only 13% of the total test time. The corrosion rate of zinc was from one to two orders higher in the salt spray phase than in any other part of the test.

When the external conditions changed, the activity of species participating in the corrosion process at the carbon steel/corrosion products interface only slowly adjusted, which was reflected by gradual changes in the corrosion rate. In contrary, zinc tended to corrode in distinct steps caused by activation of the corrosion reaction in presence of an elevated amount of chloride ions or when the relative humidity or temperature increased above certain limits. Subsequently, free chloride ions were removed from the system by binding them in stable corrosion products such as simonkolleite [28] and zinc got into a passive-like state characterized by a significant drop in the corrosion rate. In the salt spray phase, the permanent supply of chloride ions led to extreme corrosion rates.

This observation is in line with previously published results on poor prediction of zinc mass loss or time to red rust appearance for galvanized products by the normal salt spray test, NSST [21]. Although the corrosion stability of zinc coatings is at least 20-fold higher than that of carbon steel in real service conditions, comparable mass losses for zinc and carbon steel are often recorded in NSST. This can be understood in view of the current results showing the very high zinc corrosion rate in the salt spray phase. It must be pointed out that the chloride concentration in NSST as well as in VDA621-415 test is 5 wt% compared to 1 wt% in N-VDA. Any test that should reasonably mimic real service conditions has to involve shorter periods of salt contamination or lower salt loads and sufficiently long drying periods. This is in line with the recent evolution of accelerated corrosion tests for automotive materials such as the replacement of VDA 621-415 by the N-VDA (or VDA 233-102) [20].

Although the actual corrosion rate of carbon steel was not particularly elevated in the salt spray phase, the chloride contamination of the surface affects the corrosion process significantly. It is obvious when corrosion rates measured under identical climatic conditions but in sub-cycles with different time distance from the salt spray phase are compared. For example, the corrosion rate at 50 °C and at 90% RH in the sub-cycle A and in the following sub-cycle B (B_2) starting 14 and 38 h after the salt spray phase were 0.6 and 0.3 µm/h, respectively. Thus, the chloride contamination clearly accelerated the corrosion process of carbon steel. As discussed above, carbon steel showed a larger hysteresis and any equilibrium at the metal/corrosion product interface was built up relatively slowly.

Zinc reacted more readily to changes in the exposure conditions. There were periods when the corrosion rate of zinc dropped as low as 0.001 µm/h. It was shown that relatively dry periods are crucial for formation of stable corrosion products on zinc with certain protection ability. Such conditions are naturally

met in service conditions and tests with permanently high wetness generally fail to predict zinc performance in field. Although further analyses are necessary to complete the study, the available data indicate that the N-VDA test might correctly simulate real exposure conditions and provide reasonable prediction of the performance of galvanized materials.

For both carbon steel and zinc, changes in the corrosion rate were often detected when the relative humidity dropped below or increased above about 75%. It well corresponds to the deliquescence point of sodium chloride, which is 75–76% in the given temperature interval [29–31]. The deliquescence point is the relative humidity when sodium chloride forms saturated solution in equilibrium to humid air. Below this threshold level, sodium chloride is solid and thus most chloride ions are removed from the system. Diluted solution forms above the deliquescence point with a lower chloride concentration and higher film thickness.

The automated corrosion logger appears to be an interesting device for understanding the effect of technical phases (salt contamination, level of temperature or relative humidity, duration of each phase, variation between temperature and relative humidity, etc.) in accelerated corrosion tests, which may help in the development of such tests.

4 Conclusions

An automated corrosion logger allowing for real-time measurements of carbon steel and zinc corrosion rate was used in a cyclic accelerated corrosion test, N-VDA cycle. This test was selected as it offers the advantage of alternating salt spray and wet and dry cycles at temperatures from −15 up to 50 °C.

From the results, the following conclusions may be drawn:

- The ER technique proved to be a very sensitive tool for studying the corrosion kinetics of the metals. It was possible to follow changes in the corrosion rate in order of nanometers per hour. The obtained results were well reproducible and comparable to mass loss measured by metal coupons.
- The actual corrosion rate was not fully reflecting climatic conditions in the test chamber. It was affected by the exposure history due to limited rates of wetting/drying and oxygen and ion transport to the reaction interface under a layer of corrosion products. The hysteresis was particularly strong for carbon steel. Except the freezing phase, the steel corrosion rate varied in a narrow range from 0.2 to 0.6 μm/h.
- For zinc, 75% of the metal corroded in the salt spray phase and during following drying period while it represented only 13% of the total test time. The corrosion rate varied from 0.001 to 0.1 μm/h in particular phases of the cycle.
- During drying phases, the corrosion rate usually dropped when the relative humidity decreased below about 75%, i.e. close to the deliquescence point of sodium chloride.

Acknowledgements: We gratefully acknowledge the financial support by the European Commission under the Seventh Framework Programme, contract number 226539. All members of the project team are thanked for their contribution. *Fréderic Ledan* is thanked for valuable experimental support.

5 References

[1] L. Sjögren, On-line corrosion monitoring of environments for electronic equipment, *Report 2002:2*, Swedish Corrosion Institute, Stockholm, Sweden **2002**.
[2] *ASTM B 808-97*, Standard test method for monitoring of atmospheric corrosion chambers by quartz crystal microbalances, ASTM International, West Conshohocken, USA **2003**.
[3] S. Zakipour, C. Leygraf, *Br. Corros. J.* **1992**, *27*, 295.
[4] M. Forslund, C. Leygraf, *J. Electrochem. Soc.* **1997**, *144*, 113.
[5] L. Falat, US patent 5 411 890, (1995).
[6] O. Baltzersen, A. Solstad, A. Daaland, J. K. Holberg, *NDTnet* **2005**, 10.
[7] M. Ström, G. Ström, G. Strannhage, presented at *EUROCORR 2006*, Maastricht, The Netherlands, September 25–28, **2006**.
[8] G. Rannou, D. Thierry, N. Le Bozec, presented at *CORROSION 2010*, NACE, San Antonio, USA, March 14–18, **2010**, Paper 10170
[9] *ASTM G96*, Standard Guide for On-Line Monitoring of Corrosion in Plant Equipment (Electrical and Electrochemical Methods), West Conshohocken, USA: ASTM International **2008**.
[10] *ISO 11844-2*, Corrosion of metals and alloys – classification of low corrosivity of indoor atmospheres – Part 2: Determination of corrosion attack in indoor atmospheres, International Organization of Standardization, Genève, Suisse, **2005**.
[11] *Automated corrosion sensors as on-line real time process control tools (CORRLOG)*, Co-operative Research Project, 6th Framework Programme, Contract No. 0182 07, 09/2005-02/2008.
[12] *Protection of cultural heritage by real-time corrosion monitoring (MUSECORR)*, Collaborative Project, 7th Framework Programme, Contract No. 2265 39, 06/2009-05/2012.
[13] www.musecorr.eu, accessed 22/03/2012.
[14] T. Prosek, F. Dubois, M. Kouril, B. Scheffel, Y. Degres, M. Jouannic, M. Taube, M. Dubus, V. Hubert, D. Thierry, presented at *18th ICC*, Perth, Australia, November 20–24, **2011**, Paper 436.
[15] M. Dubus, M. Kouril, T.-P. Nguyen, T. Prosek, M. Saheb, J. Tate, *Stud. Conserv.* **2010**, *55*, 121.
[16] L. Vaissière, M. Ragazzini, G. Despert, N. Le Bozec, D. Thierry, presented at *EUROCORR 2011*, Stockholm, Sweden, September 4–8, **2011**, Paper 4631.
[17] N. Le Bozec, D. Thierry, P. Le Calvé, J.-P. Pautasso, presented at *EUROCORR 2011*, Stockholm, Sweden, September 4–8, **2011**, Paper 4629.
[18] T. Prosek, M. Kouril, L. R. Hilbert, Y. Degres, V. Blazek, D. Thierry, M. Ø. Hansen, *Corros. Eng. Sci. Tech.* **2008**, *43*, 129.
[19] T. Prosek, D. Thierry, M. Kouril, Y. Degres, presented at *CORROSION 2008*, NACE, New Orleans, USA, March 16–20, **2008**, Paper 08296.

[20] F. Beier, K.-H. Stellnbberger, S. Geisler, presented at *EUROCORR 2009*, Nice, France, September 6–10, **2009**, Paper 8412.
[21] N. Le Bozec, N. Blandin, D. Thierry, *Mater. Corros.* **2008**, *59*, 889.
[22] N. Le Bozec, A. Legac, D. Thierry, presented at *4th International Seminar in the field of Automotive Corrosion*, Stockholm, Sweden, May 5–6, **2010**.
[23] B. Rendhal, N. Le Bozec, presented at Eurocorr, Nice, France, September 6–10, **2009**, Paper 8395.
[24] T. Prosek, N. Larché, M. Vlot, F. Goodwin, D. Thierry, *Mater. Corros.* **2010**, *60*, 412.
[25] N. Le Bozec, A. Le Gac, D. Thierry, *Mater. Corros.* **2012**, *63*, 408.
[26] M. Stratmann, K. Hoffmann, *Corros. Sci.* **1989**, *29*, 1329.
[27] M. Stratmann, K. Bohnenkamp, T. Ramchandran, *Corrros. Sci.* **1987**, *27*, 905.
[28] T. Prosek, D. Thierry, C. Taxén, J. Maixner, *Corros. Sci.* **2007**, *49*, 2676.
[29] T. Prosek, A. Iversen, C. Taxén, D. Thierry, *Corrosion* **2009**, *65*, 105.
[30] A. Apelblat, *J. Chem. Thermodyn.* **1993**, *25*, 63.
[31] L. Greenspan, *J. Res. Nat. Bur. Stand.* **1977**, *81A*, 89.

(Received: April 27, 2012) W6655
(Accepted: May 20, 2012)